1-1-2012

Robust multipoint water-fat separation using fat likelihood analysis

Huanzhou Yu
GE Healthcare, United States

Scott B. Reeder
University of Wisconsin-Madison

Ann Shimakawa
GE Healthcare, United States

Charles A. McKenzie
Western University, cmcken@uwo.ca

Jean H. Brittain
GE Healthcare, United States

Magnetic Resonance in Medicine 67:1065–1076 (2012)

Robust Multipoint Water-Fat Separation Using Fat Likelihood Analysis

Huanzhou Yu,[1]* Scott B. Reeder,[2–5] Ann Shimakawa,[1] Charles A. McKenzie,[6–8] and Jean H. Brittain[9]

Fat suppression is an essential part of routine MRI scanning. Multiecho chemical-shift based water-fat separation methods estimate and correct for Bo field inhomogeneity. However, they must contend with the intrinsic challenge of water-fat ambiguity that can result in water-fat swapping. This problem arises because the signals from two chemical species, when both are modeled as a single discrete spectral peak, may appear indistinguishable in the presence of Bo off-resonance. In conventional methods, the water-fat ambiguity is typically removed by enforcing field map smoothness using region growing based algorithms. In reality, the fat spectrum has multiple spectral peaks. Using this spectral complexity, we introduce a novel concept that identifies water and fat for multiecho acquisitions by exploiting the spectral differences between water and fat. A fat likelihood map is produced to indicate if a pixel is likely to be water-dominant or fat-dominant by comparing the fitting residuals of two different signal models. The fat likelihood analysis and field map smoothness provide complementary information, and we designed an algorithm (Fat Likelihood Analysis for Multiecho Signals) to exploit both mechanisms. It is demonstrated in a wide variety of data that the Fat Likelihood Analysis for Multiecho Signals algorithm offers highly robust water-fat separation for 6-echo acquisitions, particularly in some previously challenging applications. Magn Reson Med 67:1065–1076, 2012. © 2011 Wiley Periodials, Inc.

Key words: water-fat separation; fat spectral peaks; fitting residual; multiecho; water-fat swap

Robust fat suppression is critical for many clinical applications of MRI. Recently, chemical-shift based multiecho water-fat separation methods have been increasingly used in routine clinical applications. These methods collect images at multiple echo times such that the different water-fat phase shifts can be used to estimate a Bo field inhomogeneity map (field map) and to separate water and fat images (1–10). Commonly two or three echoes are collected, sufficient for qualitative water-fat separation. When more echoes are collected, newer algorithms (8,11) can simultaneously estimate a T_2^* decay map (8,11,12), thereby calculating water and fat images with correction of the T_2^* decay and aiming for quantitative applications such as assessment of fatty infiltration of the liver (13–15).

Multiecho water-fat separation methods must address an intrinsic challenge of water-fat ambiguity. This problem arises due to the fact that both water and fat are modeled as a single spectral peak, and their signal behavior may appear identical in the presence of Bo off-resonance. For example, a voxel containing only fat "looks" just like a voxel containing only water that is off-resonance by −210 Hz (chemical shift) at 1.5 T. Such ambiguities often result in an incorrectly estimated Bo field map, further leading to water-fat swaps in part of the image or even the entire image.

The challenge of water-fat ambiguity is commonly addressed by assuming a slowly and smoothly varying Bo field map. Therefore, previous multiecho water-fat separation methods attempt to resolve water-fat ambiguity by enforcing field map smoothness (4,7,9,10,16–20). These algorithms are typically heuristic and based on variations of region growing algorithms, which may be sensitive to noise, the presence of artifacts and the physical characteristics of the object. Therefore, it is challenging to estimate the field map reliably in areas with drastic changes of Bo field, such as near the sinus due to air/tissue interface, near metal implants, or in the presence of iron. In particular, multiecho-per-repetition sequences are often used to collect multiple echoes in a single repetition (8,12,21–24) in scan time sensitive applications. However, the minimum echo time increment increases with increase of the desired resolution, which effectively reduces the spectral field-of-view of the field map that can be uniquely determined (18,25). As a result, it is more challenging to design a robust field map algorithm for multiecho acquisitions with high resolution imaging or at higher field strengths (e.g., 3 T). This limitation currently can lead to compromises in scan protocols.

The root cause of the water-fat ambiguity is that both water and fat are assumed to have a single resonance frequency in the spectral domain. In reality, the fat spectrum has multiple spectral peaks, which should allow for unambiguous identification of water and fat if the signals are noiseless. With a multipeak model in water-fat

[1]Applied Science Laboratory, GE Healthcare, Menlo Park, California, USA.
[2]Department of Radiology, University of Wisconsin, Madison, Wisconsin, USA.
[3]Department of Biomedical Engineering, University of Wisconsin, Madison, Wisconsin, USA.
[4]Department of Medical Physics, University of Wisconsin, Madison, Wisconsin, USA.
[5]Department of Medicine, University of Wisconsin, Madison, Wisconsin, USA.
[6]Department of Medical Biophysics, The University of Western Ontario, London, Ontario, Canada.
[7]Department of Physics, The University of Western Ontario, London, Ontario, Canada.
[8]Department of Biomedical Engineering, The University of Western Ontario, London, Ontario, Canada.
[9]Applied Science Laboratory, GE Healthcare, Madison, Wisconsin, USA.
*Correspondence to: Huanzhou Yu, Ph.D., 333 Ravenswood Ave, Bldg 307, Menlo Park, CA, 94025. E-mail: huanzhou.yu@gmail.com

Received 16 April 2011; revised 27 May 2011; accepted 15 June 2011.
DOI 10.1002/mrm.23087
Published online 12 August 2011 in Wiley Online Library (wileyonlinelibrary.com).

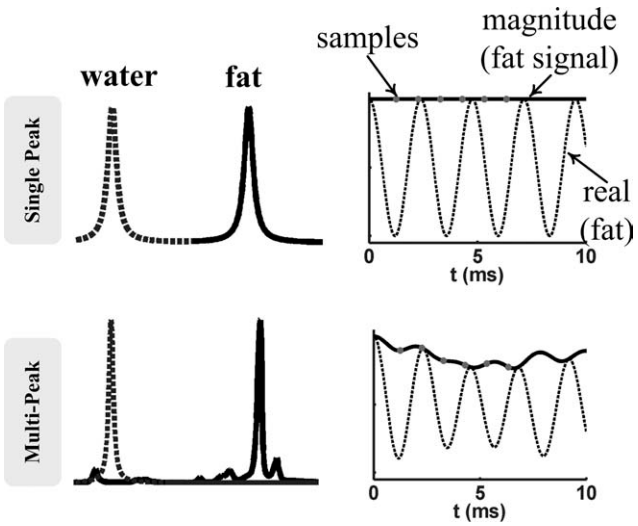

FIG. 1. Spectrum domain representation and their expected signal behaviors in the time domain for the single peak fat model and the multipeak fat model, respectively. Because of the difference in expected signal behaviors, it is possible to distinguish water and fat signals by examining which of the single peak model and the multipeak model better fit the collected signals.

separation methods (8,12), it is interesting to note that water and fat have different expected signal behaviors, as illustrated in Fig. 1. For the single peak model, the magnitude signals of either water or fat follows a flat line, while the magnitude signals of the multipeak model show oscillatory pattern due to the interaction of the fat spectral peaks with different phase evolution frequencies.

In reality, however, the signals are sampled at limited number of times. In this work, we explore the feasibility of using the revealed signal differences at six echo times to distinguish water and fat. We design a new algorithm for robust water-fat separation using the spectral difference of water and fat in addition to field map smoothness. The algorithm, based on fat likelihood analysis, is named Fat Likelihood Analysis for Multiecho Signals (FLAME). We demonstrate the effectiveness of the FLAME algorithm combined with a 6-echo acquisition and the T_2^*-IDEAL (T_2^*-Iterative Decomposition of water and fat with Echo Asymmetry and Least squares inversion) reconstruction, a water-fat separation algorithm with T_2^* estimation and correction (8) based on the IDEAL method (6).

METHODS AND MATERIALS

Fat Likelihood Analysis

As can be seen from Fig. 1, while water can be accurately characterized by a single-peak in the spectrum domain, the fat spectrum is in general more complex that consists of at least six peaks (26,27). Therefore, in the time domain, water and fat follow different signal behaviors, i.e., single-peak signal behavior for water and the multipeak signal behavior for fat. We can determine if a pixel is fat or water by examining how well the signals fit the single-peak model or the multipeak model. In the T_2^*-IDEAL method, the field map is first estimated iteratively (6). When the field map is determined, water and fat contents are uniquely determined using linear least squares inversion (6). The "goodness" of the fit can be characterized as the "residual" (R) for a field map solution $\hat{\psi}$(6,18,20), described in the following equation:

$$\mathbf{R} = \| (\mathbf{D}(\hat{\psi}) \cdot \mathrm{A} \cdot \mathrm{A}^{\dagger} \cdot \mathbf{D}(-\hat{\psi}) - \mathbf{I}) \cdot \mathbf{s} \| \quad [1]$$

where $\mathbf{I}$ is an identity matrix. $\mathbf{D}(\hat{\psi})$ is a diagonal matrix with elements of $e^{j2\pi\hat{\psi}t}$, t is a vector of echo times. $\mathbf{s}$, the signal vector, denotes the detected signals. $\mathbf{A}$ is a matrix representing the expected signal behaviors of water and fat. A^{+} represents the pseudo-inverse of the A matrix, i.e. $(\mathbf{A}^{*} \cdot \mathbf{A})^{-1} \cdot \mathbf{A}^{*}$. For the single peak model, A has the following format:

$$\mathbf{A}_{sp} = \begin{bmatrix} 1 & e^{j2\pi\Delta f\, t_1} \\ 1 & e^{j2\pi\Delta f\, t_2} \\ \cdots & \cdots \\ 1 & e^{j2\pi\Delta f\, t_N} \end{bmatrix}$$

where Δf is the chemical shift between water and fat. In the multipeak model, the fat spectrum consists of P spectral peaks, each with frequency offset Δf_p and relative amplitudes α_p ($\sum \alpha_p = 1$). Therefore, the multipeak version of the $\mathbf{A}$ matrix is:

$$\mathbf{A}_{mp} = \begin{bmatrix} 1 & \sum \alpha_p \cdot e^{j2\pi\Delta f_p\, t_1} \\ 1 & \sum \alpha_p \cdot e^{j2\pi\Delta f_p\, t_2} \\ \cdots & \cdots \\ 1 & \sum \alpha_p \cdot e^{j2\pi\Delta f_p\, t_N} \end{bmatrix}$$

In this work, a fat spectrum derived from the theoretical fat composition is used (28). Therefore, both A_{sp} and A_{mp} matrices are considered known. Finally, the corresponding residual for single peak and multipeak models are denoted as R_{sp} and R_{mp}, respectively.

The "residual" R relies on the field map value and the model used (single peak or multipeak). A small "residual" suggests that the current estimates of field map, water, and fat fit the model well. When a pixel is truly fat, the multipeak model should fit the signals better than the single peak model, i.e., $R_{\mathrm{mp}} < R_{\mathrm{sp}}$ for a field map solution that suggests the pixel to be fat dominant. On the other hand, when the pixel appears to be fat at the "swapped" solution (i.e., a truly water pixel), the single-peak model should fit the signals better than the multipeak model, i.e., $R_{\mathrm{mp}} > R_{\mathrm{sp}}$. Based on these considerations, at each pixel, we first find the field map value such that the corresponding fat content is larger than the water content (i.e., fat dominant, including fat only). We then use multipeak and single peak models to determine if this is a "true" fat pixel or a "swapped fat" pixel. This is done by calculating and comparing the residual values from single peak and multipeak models at this field map solution, leading to a "fat likelihood" index to describe the possibility of a pixel being fat based on the fitting residuals using the two models:

$$fl = \frac{R_{sp} - R_{mp}}{\max(R_{sp}, R_{mp})} \quad [2]$$

where R_{sp}, R_{mp} are the residuals of the fitting at a field map solution that leads to fat content more than the water content using the single peak model and the multipeak model, respectively.

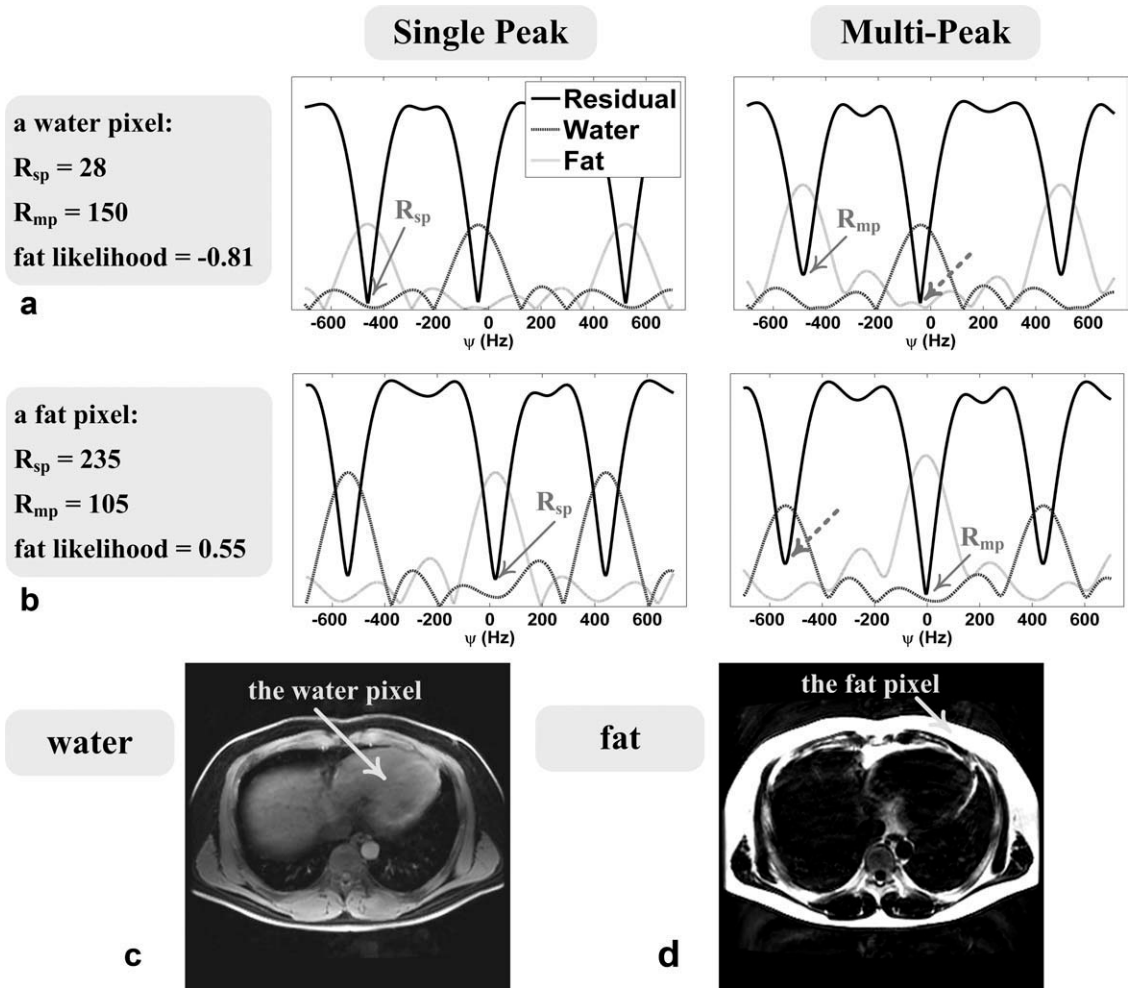

FIG. 2. Fat likelihood analysis for a typical water (**a**) and fat (**b**) pixel from a 6-echo abdominal T_2^*-IDEAL scan. For the water pixel, the single peak model fits the data better than the multipeak model (arrows), leading to a negative (−0.81) fat likelihood index. On the other hand, for the fat pixel, the multipeak model results in smaller residual than the single peak model (arrows), leading to a positive fat likelihood index (0.55). The dotted arrows point to field map values that correspond to a water pixel solution using the multipeak model (R_{mp_w} in Eq. 3), used as an alternative way to determine the fat likelihood value. The water (**c**) and fat (**d**) images are also shown for reference.

The fitting residual can be visualized on a cost-function curve (18,20). Figure 2 shows the cost function curves for a representative water and a fat pixel in a 6-echo abdominal T_2^*-IDEAL acquisition, respectively. At least two local minima appear within one period in each cost function (18,20), one is the true solution, and one is the solution of water-fat swap, as can be seen from the plot of the corresponding water/fat contents. For the water pixel, the multipeak model results in significantly higher residual at the solution that leads to the incorrect identification of a "fat pixel" ($R_{\mathrm{mp}} > R_{\mathrm{sp}}$, arrows). Therefore, the fat likelihood index calculated is a negative number (fl = −0.81), suggesting the possibility of being a water pixel. On the other hand, the multipeak model results in better fitting than the single peak model for the fat pixel (i.e., $R_{\mathrm{mp}} < R_{\mathrm{sp}}$, arrows). As a result, the fat likelihood index is a positive number (fl = 0.55). In general, a fat likelihood index approaching 1 suggests the strong possibility of a fat pixel, while a value approaching −1 suggests the strong possibility of a water pixel.

Alternatively, the fat likelihood value can be obtained by directly comparing the residuals of the neighboring two local minima when using the multipeak model:

$$fl = \frac{R_{mp\_w} - R_{mp\_f}}{\max(R_{mp\_w}, R_{mp\_f})} \quad [3]$$

Here, R_{mp_w} represents the residual calculated at the field map value corresponding to a water pixel with the multipeak model (dashed arrow in Fig. 2), while R_{mp_f} denotes the residual calculated at the field map value corresponding to a fat pixel with the multipeak model (=R_{mp} in Eq. 2). In general, Eq. 2 results in close values as Eq. 3 because in certain circumstances $R_{mp\_w} = R_{sp}$ (ignoring noise), for example, when the pixel contains only fat or water. In this work, we will use formulation based on Eq. 3 as it involves the T_2^* IDEAL iterative field map calculation of only one signal model (multipeak) and is significantly faster than the calculation based on Eq. 2.

Fat Likelihood Map

The fat likelihood analysis can be performed on a pixel-by-pixel basis for the entire image, leading to a fat

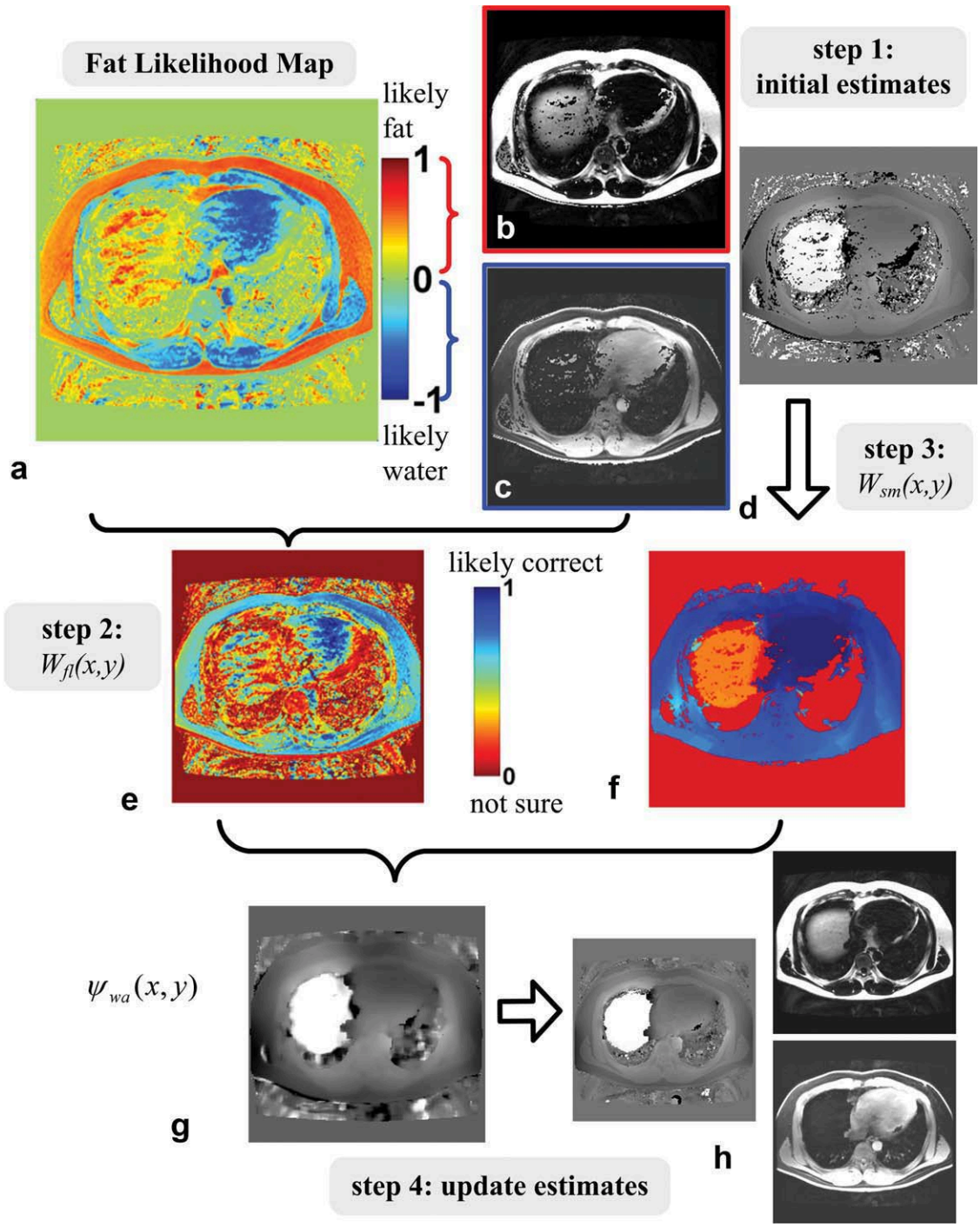

FIG. 3. Flow diagram of the FLAME algorithm. The pixel-by-pixel fat likelihood analysis produces a fat likelihood map (**a**), based on which, initial estimates of fat (**b**), water (**c**) and field map (**d**) are made in "step 1." Two weighting maps are then generated based on the fat likelihood analysis (**e**, "step 2") and the characterization of the field map smoothness (**f**, "step 3"). In step 4, an averaged field map (**g**) is calculated, where the local averaging is weighted by the two weighting maps. Finally, the initial estimates are updated (**h**). This completes one iteration. Note that the majority part of the water-fat swap appeared in the initial estimate (dome of liver) remains. Steps 2–4 are repeated until no pixel needs to be updated. [Color figure can be viewed in the online issue, which is available at wileyonlinelibrary.com.]

likelihood map, as shown in Fig. 3a. In this fat likelihood map, a value close to 1 (red) suggests high likelihood of being a fat pixel, whereas a value close to −1 (blue) suggests high likelihood of being a water pixel. The fat likelihood map is in general very consistent with the actual distribution of water and fat (Fig. 2c,d). It is important to note that the fat likelihood map is generated independent of the field map and is therefore fundamentally different from conventional field map based methods.

One approach to use the fat likelihood map is to identify all pixels with positive fat likelihood values as fat-dominant, while all pixels with negative values as

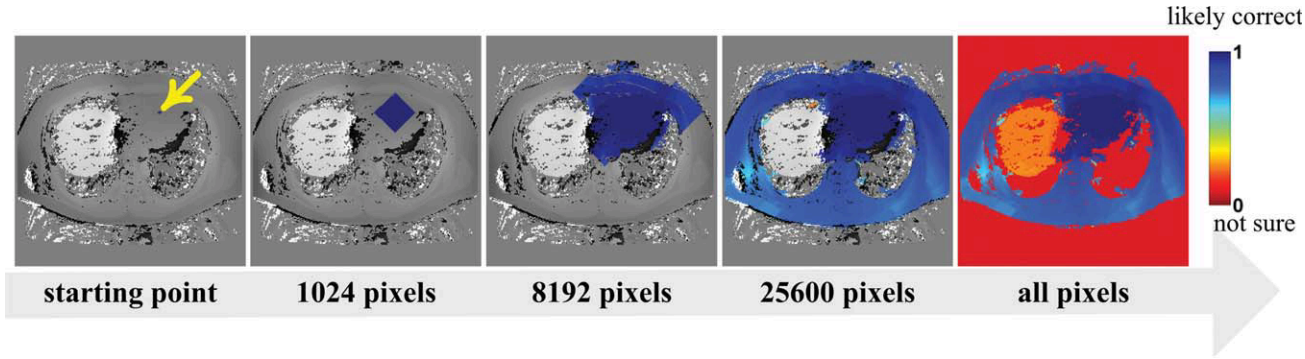

FIG. 4. Multiple iterations of the process to generate the weighting map ($W_{sm}(x,y)$) by characterizing field map smoothness. The trajectory starts from the pixel with the highest $W_{fl}(x,y)$ value (arrow), then follows the slowest field map gradient direction for the next pixel. The $W_{sm}(x,y)$ value is determined from the averaged $W_{sm}(x,y)$ in its neighborhood, deducted by an amount scaled with the field map changes between the current pixel and its neighbors. Therefore, the $W_{sm}(x,y)$ maintains its value in areas with smooth field map variation (blue), while loses its value rapidly when the field map experiences sharp transitions. As a result, the areas with correct field map estimation are labeled with high values (blue) while the areas with possible water-fat swap (e.g., the dome of the liver) are labeled with low values (red). [Color figure can be viewed in the online issue, which is available at wileyonlinelibrary.com.]

water-dominant. The results are shown in Fig. 3b,c. Despite the fact that majority pixels are correctly identified, there are small areas of pixels that are mislabeled, for example at the dome of the liver. The remaining water-fat swaps typically happen in places where the fat likelihood map shows a low probability of being either water or fat. This uncertainty comes from the presence of noise, artifact, rapid T_2^* decay or inaccuracies in the spectral modeling of fat. This approach makes binary decision based on the fat likelihood maps, without differentiation between pixels having high confidence (high likelihood value) and pixels having high uncertainty (small likelihood value). To address this concern, we introduce an algorithm for robust identification of water and fat that takes advantage of the rich information of the fat likelihood map using the approach of "weighting maps." The field map smoothness is also taken into consideration as it provides valuable complementary information. The overall flow is shown in Fig. 3 using abdominal data as an example.

Step 1: Initial Estimates of Water, Fat, and Field Map

The water and fat images shown in Fig. 3b,c serve as an excellent first estimate. The corresponding field map is also determined. At each pixel, the field map solution that leads to the identification of water and fat consistent with the fat likelihood value (i.e., Fig. 3b,c) is used as the initial estimate for that pixel. For example, for the water pixel shown in Fig. 2a, the chosen field map value is −40 Hz. Similarly, for the fat pixel shown in Fig. 2b, a value of −4 Hz is assigned. This pixel-by-pixel process leads to Fig. 3d, the initial estimate of the field map.

Step 2: Produce a Weighting Map Based on Fat Likelihood Analysis

As mentioned previously, the initial estimates come from the binary decision of the fat likelihood map. To take advantages of the inherent full range of the fat likelihood values, a weighting map based on the fat likelihood analysis ($W_{fl}(x,y)$) is produced by simply taking the absolute values of the fat likelihood map, as shown in Fig. 3e. This weighting map describes how confident we are with the initial estimates (Fig. 3b–d) based on fat likelihood analysis. A high value in $W_{fl}(x,y)$ (close to 1 or blue in Fig. 3e) suggests that the initial estimates are very likely to be correct, while a low weight (close to 0 or red in Fig. 3e) represents low confidence in the current estimates.

Step 3: Produce a Second Weighting Map by Characterizing Field Map Smoothness

The FLAME algorithm still uses the field map smoothness as a complementary source of information beyond the fat likelihood analysis. For a given estimate of the field map, we introduce an algorithm to characterize the field map smoothness, producing a second weighting map: $W_{sm}(x,y)$. The final $W_{sm}(x,y)$ is shown in Fig. 3f, while the process of generating such a weighting map is illustrated in Fig. 4. First, a "seed" pixel (x_maxc,y_maxc) is identified by selecting the pixel with the highest confidence in $W_{fl}(x,y)$ in step 2 (arrow in Fig. 4a). A value of 1 is assigned to the $W_{sm}(x,y)$ value for this seed pixel (i.e., $W_{sm}(x\_maxc,y\_maxc)=1$).

The algorithm then follows the slowest gradient in the field map to select the next pixel (4). For each pixel along this minimum field map gradient trajectory, the $W_{sm}(x,y)$ value is calculated based on the $W_{sm}(x,y)$ values of neighboring pixels that have been already determined:

$$W_{sm}(x,y)=\frac{\sum_n W_{sm}(x_n,y_n)\cdot|s(x_n,y_n)|\cdot e^{-f\cdot(\psi(x,y)-\psi(x_n,y_n))^2}}{\sum_n|s(x_n,y_n)|} \quad [4]$$

where (x_n, y_n) indicates the neighboring pixels of the pixel (x, y). In our implementation, the "neighbor" is defined as all pixels in a kernel of 15 × 15 pixels. The averaging of $W_{sm}(x,y)$ is weighted by the signal strength ($|s(x_n,y_n)|$) and the field map difference between the current pixel ($\psi(x, y)$) and the neighboring pixels ($\psi(x_n,$

y_n)). Therefore, the $W_{sm}(x,y)$ value of the current pixel can be considered as the average of $W_{sm}(x,y)$ values at the neighboring pixels reduced by an amount that increases with the field map difference between those pixels. Therefore, $W_{sm}(x,y)$ loses its value slowly when the field map varies slowly, while $W_{sm}(x,y)$ drops rapidly when the field map experiences sharp jumps, which typically indicate a water-fat swap. f is a "friction factor" that controls how fast the $W_{sm}(x,y)$ loses its value. $W_{sm}(x,y)$ is more sensitive to the field map variation with a bigger "friction factor." In our implementation, f is selected empirically such that there is sufficient contrast in $W_{sm}(x,y)$ values between correctly and incorrectly estimated field map areas (Δf is the chemical shift frequency):

$$f = \frac{4}{\Delta f^2} \quad [5]$$

Snap-shots of multiple steps illustrating the process of generating $W_{sm}(x,y)$ are shown in Figure 4. Like $W_{fl}(x,y)$, a value close to 1 represents areas with high confidence (smooth field map variation), while a value close to 0 indicates regions with possible water-fat swap.

Step 4: Update the Estimates Using the Two Weighting Maps

In both weighting maps ($W_{fl}(x,y)$ and $W_{sm}(x,y)$), large values suggest high confidence in the current estimates, whereas low values suggest a high likelihood of a water-fat swap. Therefore, the weighting maps can be used to find those pixels with possible water-fat swaps and recalculate their field map values. This is achieved by first calculating a locally averaged field map (ψ_{wa}), weighted by the signal strength and the two weighting maps.

$$\psi_{wa}(x,y) = \frac{\sum_n \psi(x_n,y_n)\cdot|s(x_n,y_n)|\cdot W_{fl}(x_n,y_n)\cdot W_{sm}(x_n,y_n)}{\sum_n |s(x_n,y_n)|\cdot W_{fl}(x_n,y_n)\cdot W_{sm}(x_n,y_n)} \quad [6]$$

At the boundary of possible water-fat swap, those pixels with higher weights contribute to the averaging substantially more than those with less weights. Therefore, the correctly estimated field map is able to "penetrate" into those incorrectly estimated areas, as shown in Fig. 3g.

Finally, ψ_{wa} is compared with the current field map estimate ψ. At pixels with substantial difference, the field map is recalculated using ψ_{wa} as the initial guess. This process ensures the growth of the correctly estimated areas, as shown in Fig. 3h with the water and fat estimates also updated.

This completes one iteration. Figure 3h then replaces the initial estimates (Fig. 3b–d), followed by more iterations, where steps 3 and 4 are repeated, until no pixel needs to be recalculated in step 4.

RESULTS

Figure 5 presents the intermediate and final results of applying the FLAME algorithm to the 6-echo abdominal scan of a healthy volunteer shown earlier in Figs. 2–4. This 6-echo scan was acquired at 3 T with echo time, TE_1 = 1.3 ms, ΔTE = 1.0 ms (0.86π in phase shift between water and fat) and parallel imaging acceleration factor of 2.2. A superior slice was chosen as a challenging case, where there is often big field map variation at the dome of the liver due to the air-tissue interface. Throughout the iterations, $W_{sm}(x,y)$ was updated and accurately captured the boundary between the correctly estimated and swapped areas. The two weighting maps drove the improvement of the next iteration, and the area with incorrect estimates continuously eroded. In 21 iterations, correctly separated water, fat, and field map were obtained.

Figure 6 shows results from a 6-echo abdominal scan at 3 T with TE_1 = 1.2 ms, ΔTE = 1.5 ms (1.3π of phase shift between water and fat). Such a long echo spacing is challenging for traditional methods, because it effectively reduces the sampling rate in the spectral domain, leading to a smaller range of field map that can be unambiguously determined. In T_2^*-IDEAL acquisitions with equally spaced echoes, the field map solutions are periodic with the period inversely proportional to the echo spacing (18). Therefore, the local minima are closer to the true solution with longer echo spacing scans, and thus they are more difficult to discriminate. With the FLAME algorithm, the fat likelihood map (Fig. 6a) accurately predicted the water-fat distribution, leading to an excellent initial water-fat separation (Fig. 6b,c). Only a few more iterations were required to obtain a correct water-fat separation (Fig. 6d). For comparison, the water-fat separation from a field map based region growing algorithm (20) is also shown in Fig. 6e. A water-fat swap occurred in the right lobe of the liver, where the incorrectly estimated field map appears smooth with respect to the field map values nearby in subcutaneous fat, making it particularly challenging for conventional field map based methods.

Robust water-fat separation in the presence of unconnected, discontinuous tissues has always been challenging for region growing based algorithms, as region growing may be inadequate when the trajectory traverses through the noise regions between tissue segments. Figure 7 shows such a challenging slice in a coronal head-neck-shoulder acquisition at 3 T with TE_1 = 1.2 ms, ΔTE = 1 ms (0.84π of phase shift between water and fat). While the conventional region growing technique (Fig 7e) worked well in the shoulder area, it resulted in a complete swap of water and fat in the head area. With the FLAME algorithm, the fat likelihood map (Fig. 7a) and the derived $W_{fl}(x,y)$ (Fig. 7b) are generated on a pixel-by-pixel-basis, and therefore are fundamentally insensitive to the tissue connections, providing an excellent set of initial estimates (Fig. 7c). Despite the fact that the $W_{sm}(x,y)$ only provided useful weighting in the head area, the algorithm was still able to rely on the $W_{fl}(x,y)$ in the shoulder area for accurate water-fat identification. The FLAME algorithm is promising for isolated tissue "islands" because the $W_{fl}(x,y)$, which exploits spectral differences between water and fat, and the $W_{sm}(x,y)$, which exploits field map smoothness, are complementary and independent mechanisms that can be used to avoid water-fat swapping.

Water-fat separation in the presence of iron overload is also a challenging application. Figure 8 presents results

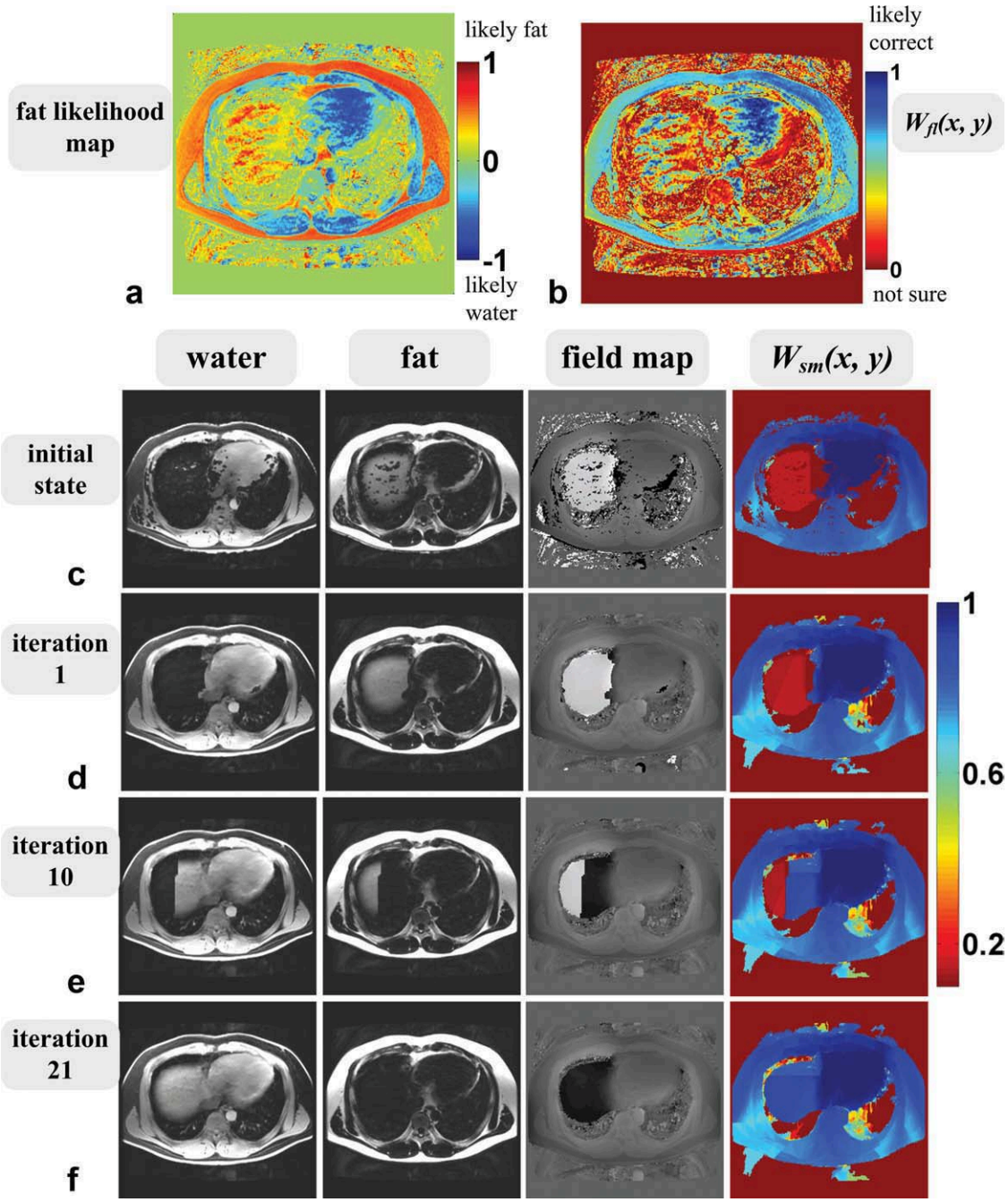

FIG. 5. Intermediate images (**c–e**) and the final results (**f**) of applying FLAME algorithm to the 6-echo abdominal scan shown in Figs. 2–4. For convenience, the fat likelihood map (**a**) and the weighting map $W_{fl}(x,y)$ (**b**) are also included. [Color figure can be viewed in the online issue, which is available at wileyonlinelibrary.com.]

from a liver patient with severe iron overload (1.5 T, TE_1 = 1.0 ms, ΔTE = 1.6 ms or 0.67π of phase shift between water and fat). The R_2^* map from T_2^*-IDEAL is shown in Fig. 8f. T_2^* measured in the liver is approximately 1.4 ms, significantly shorter than the normal range of T_2^* (> 20 ms (29)). As a result, the liver signals decay away rapidly, diminishing SNR with the increase of echo times. The noisy and erroneous estimate of the field map in the liver is propagated to the nearby subcutaneous fat area due the region growing process, causing water-fat swapping, even in areas with reasonable SNR (Fig. 8e). The FLAME algorithm resulted in an accurate fat likelihood map (Fig. 8a). In liver, fat likelihood values are close to zero due to lack of SNR to support a confident decision. Despite this uncertainly, the initial estimates from the FLAME algorithm correctly decomposed water and fat in areas outside liver, including subcutaneous fat (Fig. 8c). These high confidence pixels helped the estimation of the liver pixels in later iterations, and correct water-fat separation was obtained after nine iterations (Fig. 8d).

Finally, results from a patient with significant hepatic fatty infiltration are shown in Figure 9 (1.5 T, TE_1 = 1.2 ms, ΔTE = 2.0 ms or 0.84π of phase shift between water and fat). The fat likelihood map (Fig. 9a) is in good

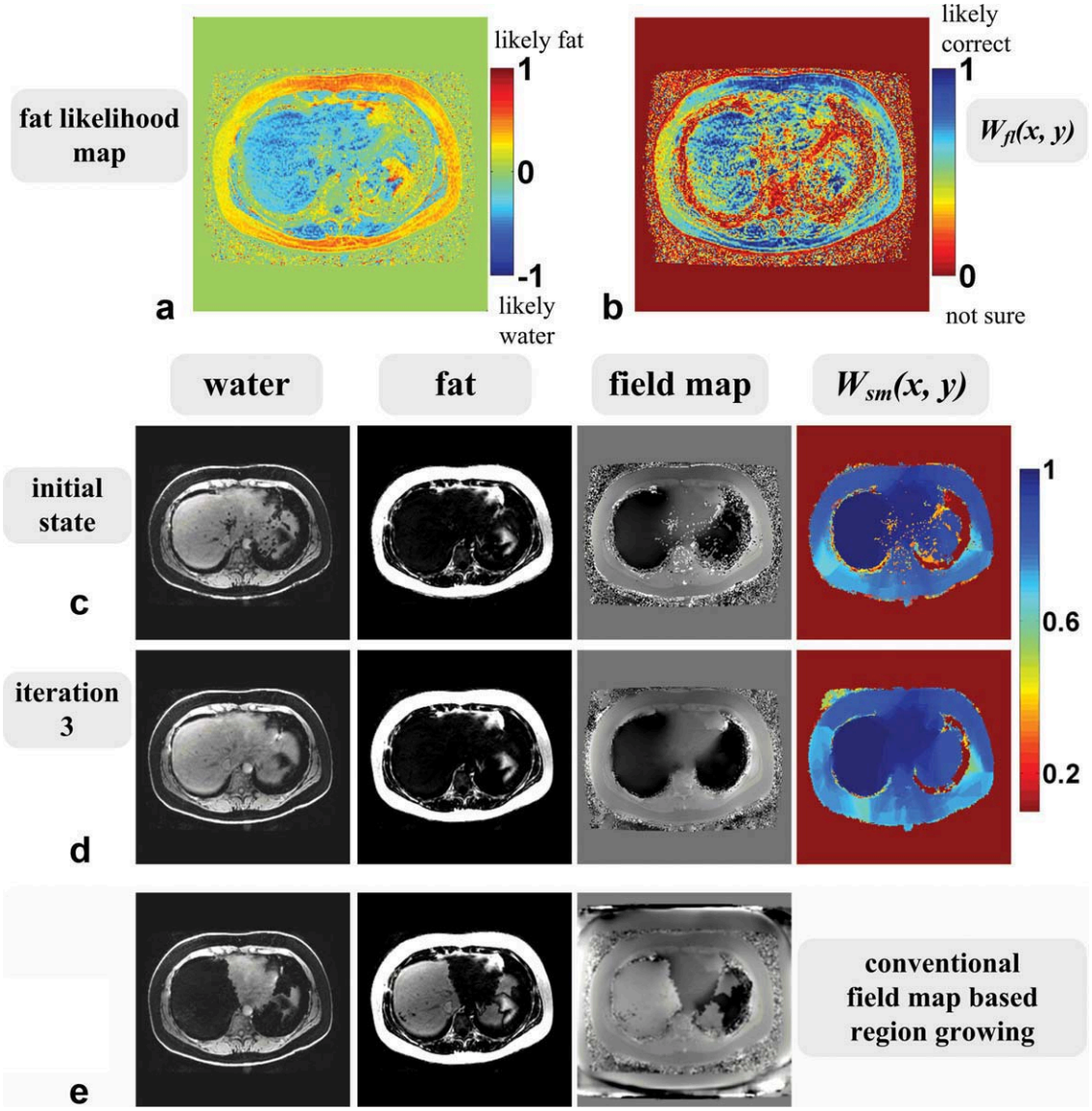

FIG. 6. Results from a scan with long echo spacing ($TE_1 = 1.2$ ms, $\Delta TE = 1.5$ ms or 1.3π in water-fat phase shift) at 3 T. The fat likelihood map (**a**) is in close agreement with the actual water-fat distribution, leading to a high quality $W_{fl}(x,y)$ (**b**) and the initial estimates (**c**). A successful water-fat separation was obtained after only three iterations (**d**). Such a long echo spacing is challenging for a traditional field map based region growing algorithm, which resulted in water-fat swaps (**e**). [Color figure can be viewed in the online issue, which is available at wileyonlinelibrary.com.]

agreement with the true distribution of water and fat, leading to a reliable $W_{fl}(x,y)$ (Fig. 9b) and excellent initial estimates (Fig. 9c). Because of the highly accurate initial estimates, a uniform water-fat decomposition was achieved after only one iteration (Fig. 9d).

DISCUSSION

Field map estimation is a critical step in multiecho chemical shift based water-fat separation methods. It often suffers from an intrinsic ambiguity problem, where incorrectly estimated field map values can lead to water-fat swaps. Conventional water-fat separation methods rely on enforcing field or phase smoothness to resolve this water-fat ambiguity. In this work, we introduce a novel approach to identify water and fat by exploiting the spectral complexity of fat. A fat likelihood map is produced to indicate whether a pixel is likely to be water-dominant or fat-dominant on a pixel-by-pixel basis, completely independent of field map estimation. The fat likelihood analysis and field map smoothness provide complementary information, and we designed an algorithm (FLAME) to take advantage of both mechanisms. FLAME relies largely on pixel independent processing, and therefore is fundamentally less sensitive to the complexity of the imaged objects. Minimizing the dependence on region growing also prevents errors from spreading to other parts of the image. The fat likelihood map is not susceptible to an incorrect center frequency, a situation that may occur when imaging fat dominant anatomy. Finally, it is demonstrated that the FLAME algorithm may offer reliable water fat separation for scans with long echo spacing scans. Such scans are hindered by increasing difficulty in discriminating the local

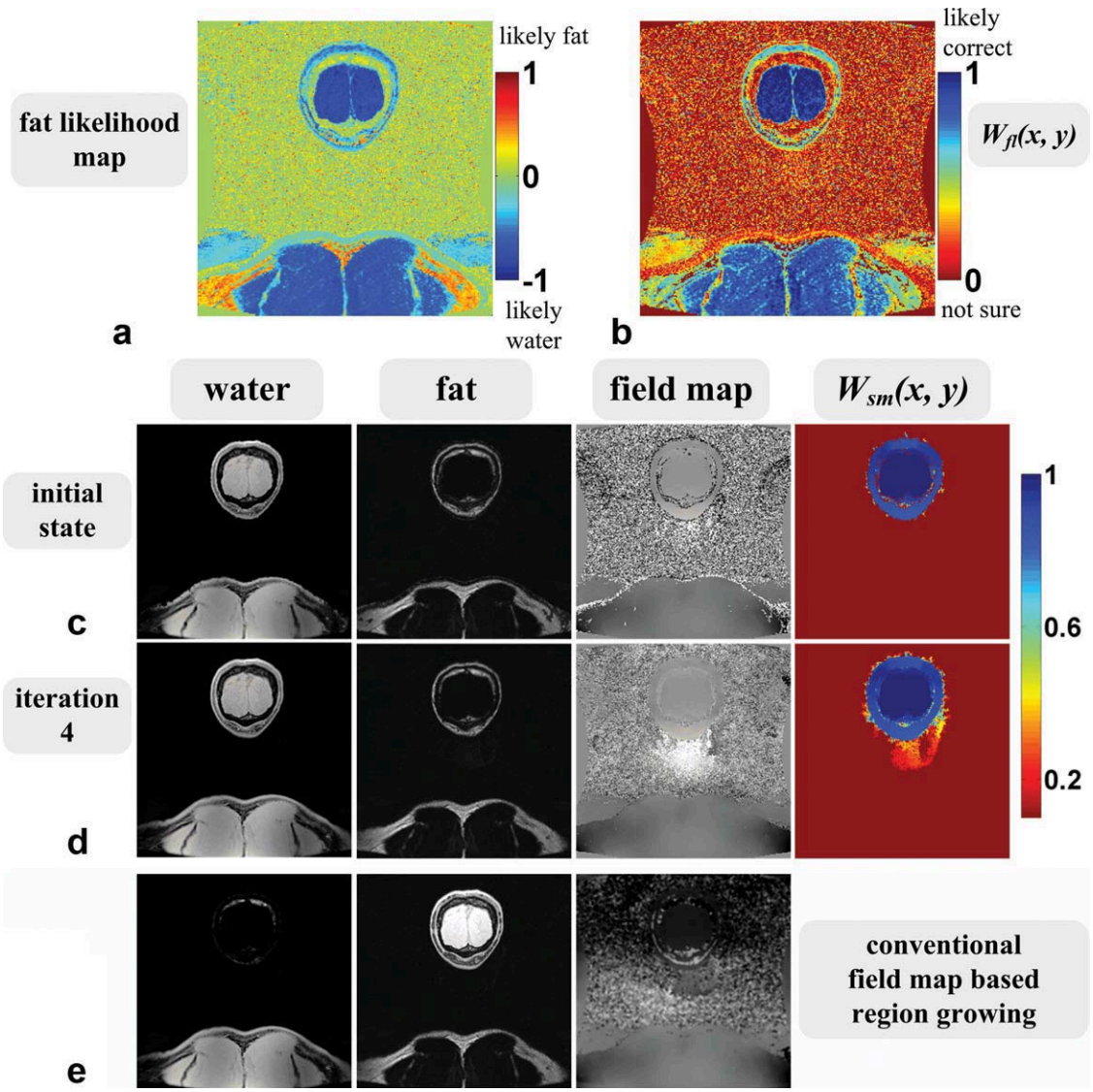

FIG. 7. Results from a 6-echo scan at 3 T to demonstrate the robust water-fat separation using FLAME when there are disconnected tissue areas. The fat likelihood map (**a**) and the derived $W_{fl}(x,y)$ (**b**) were generated on a pixel-by-pixel basis, therefore are fundamentally insensitive to tissue connections, leading to excellent the initial estimates (**c**) in both head and shoulder tissue areas. A correct water-fat separation was obtained after only four iterations (**d**). The conventional field map based region growing method suffered from water-fat swap in the head area (**e**). [Color figure can be viewed in the online issue, which is available at wileyonlinelibrary.com.]

minima from the true solution (18,20). In the past, compromises have been made by, for example, reducing the spatial resolution or interleaving multiple multiecho sequences (30) which inevitably increases the scan time. Therefore, improving the robustness of the long echo spacing scans may enable water-fat separation in previously challenging applications, including at high field strengths, in high spatial resolution, and scan time sensitive applications.

Many factors can affect the accuracy of the fat likelihood maps, including the presence of noise, artifacts, or phase errors that could change the residual relationship between the true solution and local minima. In particular, how well the difference between the single peak and multipeak signal behaviors can be "observed" varies with the T_2^* decay. In the presence of extremely rapid T_2^* decay, the signal difference between the models becomes increasingly difficult to measure, making the accuracy of the fat likelihood value more sensitive to noise, artifacts or phase errors. The fat spectrum is assumed to be known, including the frequency and the relative amplitude of the peaks. We have used a model derived from the theoretical composition of fat (28). However, we found the fat likelihood maps often appear similar even when using different fat spectral models. An example is shown in Figure 10. Fat likelihood maps of an abdominal slice are calculated based on three different fat spectra: the default fat spectrum reported by Hamilton et al. (28) and used in this work, a fat spectrum based on a scan in a vegetable oil phantom (11), and a self-calibrated fat spectrum derived from 6-echo data (11). All fat likelihood maps are in excellent agreement with the water-fat distribution. Performing the FLAME algorithm with any of these spectra leads to successful decomposition of water and fat.

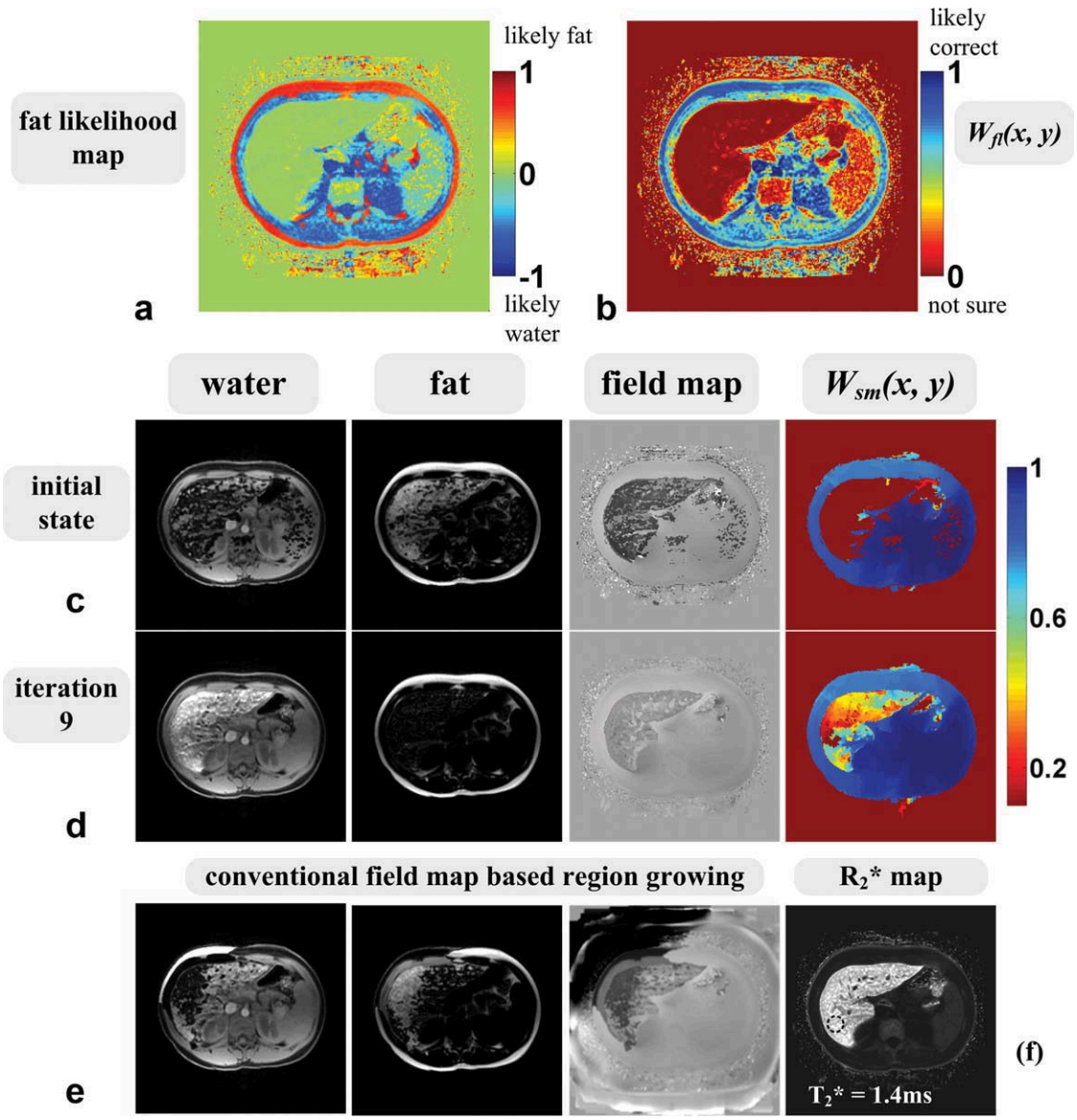

FIG. 8. Results from a 6-echo scan at 1.5 T in a patient with severe hepatic iron overload. The fat likelihood map (**a**) and the $W_{fl}(x,y)$ (**b**) provided accurate water-fat identification outside of the liver, while showed high uncertainty in liver due to the lack of signals. Nonetheless, the quality of the initial estimates (**c**) was adequate for the algorithm to complete in nine iterations (**d**). In contrast, the region growing method suffered from the poor SNR in the liver. The errors were propagated to the subcutaneous fat region, resulting in substantial water-fat swap in both inside and outside the liver (**e**). The map (**f**) from T_2^*-IDEAL reconstruction suggests high level of iron concentration in liver ($T_2^* = 1.4$ ms). [Color figure can be viewed in the online issue, which is available at wileyonlinelibrary.com.]

In addition, the accuracy of the fat likelihood map may be sensitive to the number of echoes used. Intuitively, the difference between the single peak and multi-peak signal behaviors is better revealed when more echoes are collected (i.e., longer "observation window"), leading to more accurate fat likelihood maps. Future work will attempt to understand the sensitivity of the fat likelihood accuracy on the number of echoes. In particular, applying FLAME to a 3-pt acquisition will be explored and optimized. We have illustrated the FLAME algorithm primarily using water-only and fat-only pixels as examples. However, the fat likelihood analysis also applies to pixels with mixed concentration of water and fat. In fact, the local minima of the mixed pixels are associated with larger residuals even in the single peak modeling (20), therefore, the fat likelihood values are more accurate when water and fat are mixed. This is the motivation behind some algorithms that explore low-resolution reconstructions (18,31,32) for robust field map estimation, an approach FLAME can also use to improve the robustness.

The FLAME algorithm can be implemented with great computational efficiency. In our approach, the two possible field map solutions are found through T_2^*-IDEAL Gauss-Newton iterations (6) at each pixel during the initialization step. As a result, during the following steps (steps 2–4 in Fig. 2), no Gauss-Newton iteration needs to be performed, while the proper field map can simply be

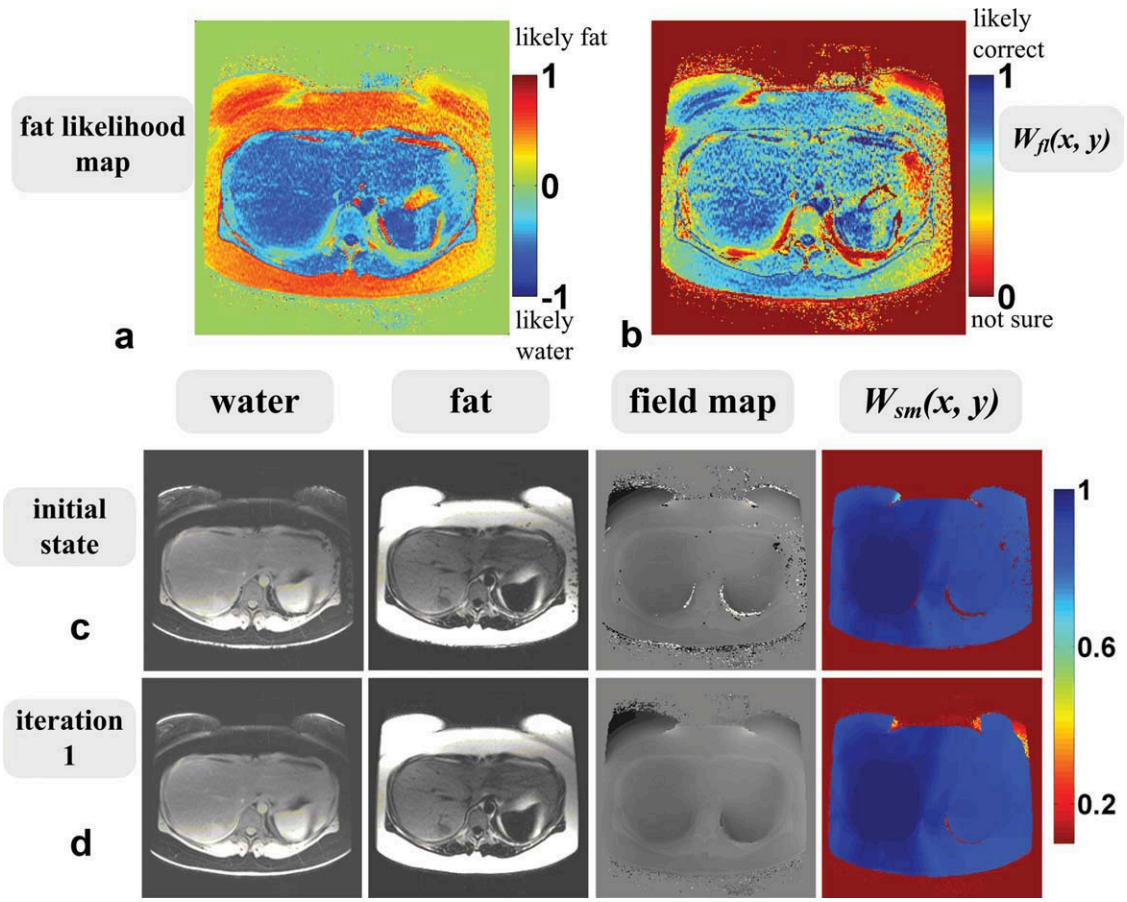

FIG. 9. Results from a 6-echo scan at 1.5 T in a patient with 40% hepatic fatty infiltration measured from T_2^*-IDEAL. The fat likelihood map (**a**) is in excellent agreement with the actual water-fat distribution, leading to highly accurate $W_{fl}(x,y)$ (**b**) and initial estimates (**c**). It required only one iteration to obtain the final and uniform water-fat separation (**d**). [Color figure can be viewed in the online issue, which is available at wileyonlinelibrary.com.]

picked from the initialized candidates, taking into considerations that the field map solutions are periodic (18). Alternatively, it may be possible to calculate the field map candidates using an algebraic formulation (17) or other nonlinear estimation methods (9,16), completely eliminating the need for the Gauss-Newton iterations. Furthermore, deriving $W_{fl}(x,y)$ from the fat likelihood map involves minimal computation (flip of the signs), while $W_{sm}(x,y)$ can be updated from iteration to iteration efficiently as the trajectory remains the same until it hits a pixel whose field map value has changed. Finally, not all pixels need to be evaluated at every iteration. Only those pixels that are close to a pixel that has changed field map value need to be evaluated. Therefore, fewer and fewer pixels are visited with increasing iterations. For our implementation, most computation is spent in initialization of

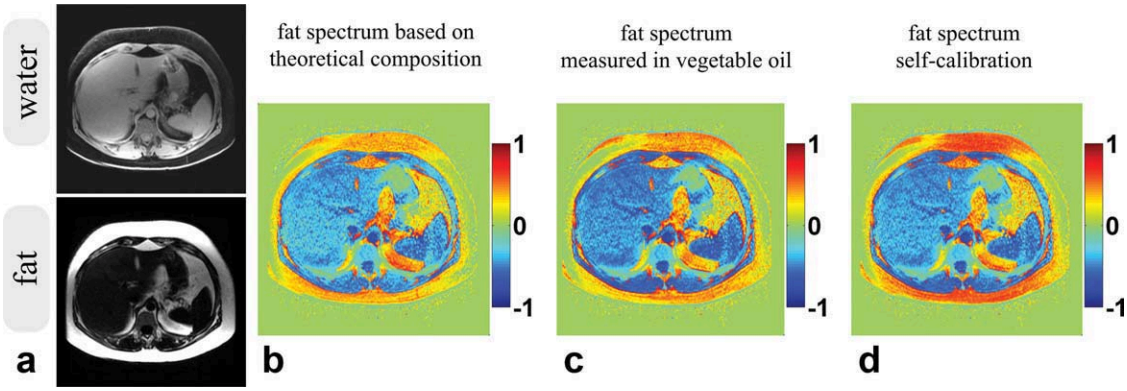

FIG. 10. Fat likelihood maps (**b**, **c**, **d**) using three different fat spectra in a 6-echo scan at 1.5 T show substantial similarities, demonstrating that FLAME algorithm generally does not require highly precise fat spectrum modeling. Water and fat images are shown for reference (**a**). [Color figure can be viewed in the online issue, which is available at wileyonlinelibrary.com.]

the fat likelihood map, which is roughly the same as performing pixel-independent T_2^*-IDEAL twice but without region growing (20). The fat likelihood map is processed on a pixel-by-pixel basis and thus can be greatly accelerated using multicore computation platforms.

In this work, T_2^*-IDEAL is used to demonstrate the FLAME algorithm. However, the concept of the fat likelihood analysis can be applied in a variety of water-fat separation techniques that allow the evaluation of fitting residuals using single peak and multipeak models. Various approaches may be explored to make the water and fat spectra more distinct from each other, e.g., preparation pulses or collecting additional low resolution echoes. FLAME may be applied in fat quantification algorithms that are based on the magnitude signals (12). In such "magnitude-based" algorithms, phase information is discarded and thus the field map is not estimated. Therefore, water-fat ambiguity is not resolved and fat-fraction can only be uniquely determined in a 50% range. By evaluating the fitting residuals using the single peak and multipeak models, it is possible to generate a fat likelihood map, potentially achieving a full 0–100% range using the magnitude-based methods. Finally, the FLAME algorithm can be easily extended to 3D, further improving its efficiency and robustness.

In conclusion, we introduced a novel approach for reliable identification of water and fat by exploiting their spectral differences. It adds another useful dimension to improve the robustness of multiecho water-fat separation methods in addition to conventional field map based approaches. We have described a new algorithm, FLAME, that combines the strength of both the spectral analysis and field map smoothness mechanisms. Results were demonstrated in a wide variety of data showing that the FLAME algorithm offers highly robust water-fat separation for 6-echo acquisitions, particularly in some previously challenging applications.

REFERENCES

1. Dixon WT. Simple proton spectroscopic imaging. Radiology 1984; 153:189–194.
2. Glover GH. Multipoint Dixon technique for water and fat proton and susceptibility imaging. J Magn Reson Imaging 1991;1:521–530.
3. Glover GH, Schneider E. Three-point Dixon technique for true water/fat decomposition with B0 inhomogeneity correction. Magn Reson Med 1991;18:371–383.
4. Ma J. Breath-hold water and fat imaging using a dual-echo two-point Dixon technique with an efficient and robust phase-correction algorithm. Magn Reson Med 2004;52:415–419.
5. Ma J, Singh SK, Kumar AJ, Leeds NE, Broemeling LD. Method for efficient fast spin echo Dixon imaging. Magn Reson Med 2002;48:1021–1027.
6. Reeder SB, Wen Z, Yu H, Pineda AR, Gold GE, Markl M, Pelc NJ. Multicoil Dixon chemical species separation with an iterative least-squares estimation method. Magn Reson Med 2004;51:35–45.
7. Xiang QS, An L. Water-fat imaging with direct phase encoding. J Magn Reson Imaging 1997;7:1002–1015.
8. Yu H, McKenzie CA, Shimakawa A, Vu AT, Brau AC, Beatty PJ, Pineda AR, Brittain JH, Reeder SB. Multiecho reconstruction for simultaneous water-fat decomposition and T_2^* estimation. J Magn Reson Imaging 2007;26:1153–1161.
9. Hernando D, Haldar JP, Sutton BP, Ma J, Kellman P, Liang ZP. Joint estimation of water/fat images and field inhomogeneity map. Magn Reson Med 2008;59:571–580.
10. Xiang QS. Two-point water-fat imaging with partially-opposed-phase (POP) acquisition: an asymmetric Dixon method. Magn Reson Med 2006;56:572–584.
11. Yu H, Shimakawa A, McKenzie CA, Brodsky E, Brittain JH, Reeder SB. Multiecho water-fat separation and simultaneous estimation with multifrequency fat spectrum modeling. Magn Reson Med 2008;60:1122–1134.
12. Bydder M, Yokoo T, Hamilton G, Middleton MS, Chavez AD, Schwimmer JB, Lavine JE, Sirlin CB. Relaxation effects in the quantification of fat using gradient echo imaging. Magn Reson Imaging 2008;26:347–359.
13. Hussain HK, Chenevert TL, Londy FJ, Gulani V, Swanson SD, McKenna BJ, Appelman HD, Adusumilli S, Greenson JK, Conjeevaram HS. Hepatic fat fraction: MR imaging for quantitative measurement and display—early experience. Radiology 2005;237:1048–1055.
14. Kim H, Taksali SE, Dufour S, Befroy D, Goodman TR, Petersen KF, Shulman GI, Caprio S, Constable RT. Comparative MR study of hepatic fat quantification using single-voxel proton spectroscopy, two-point dixon and three-point IDEAL. Magn Reson Med 2008;59:521–527.
15. Reeder SB, Robson PM, Yu H, Shimakawa A, Hines CD, McKenzie CA, Brittain JH. Quantification of hepatic steatosis with MRI: the effects of accurate fat spectral modeling. J Magn Reson Imaging 2009; 29:1332–1339.
16. Hernando D, Kellman P, Haldar JP, Liang ZP. Robust water/fat separation in the presence of large field inhomogeneities using a graph cut algorithm. Magn Reson Med 2010;63:79–90.
17. Jacob M, Sutton BP. Algebraic decomposition of fat and water in MRI. IEEE Trans Med Imaging 2009;28:173–184.
18. Lu W, Hargreaves BA. Multiresolution field map estimation using golden section search for water-fat separation. Magn Reson Med 2008;60:236–244.
19. Schmidt MA, Fraser KM. Two-point Dixon fat-water separation: improving reliability and accuracy in phase correction algorithms. J Magn Reson Imaging 2008;27:1122–1129.
20. Yu H, Reeder SB, Shimakawa A, Brittain JH, Pelc NJ. Field map estimation with a region growing scheme for iterative 3-point water-fat decomposition. Magn Reson Med 2005;54:1032–1039.
21. Koken P, Eggers H, Bornert P. Fast single breath-hold 3D abdominal imaging with water-fat separation. Proceedings 14th Scientific Meeting, International Society for Magnetic Resonance in Medicine. Berlin, Germany; 2007. p 1623.
22. Lu W, Yu H, Shimakawa A, Alley M, Reeder SB, Hargreaves BA. Water-fat separation with bipolar multiecho sequences. Magn Reson Med 2008;60:198–209.
23. Wieben O, Leupold J, Mansson S, J H. Multi-echo balanced SSFP imaging for iterative Dixon reconstruction. Proceedings 12th Scientific Meeting, International Society for Magnetic Resonance in Medicine. Miami, Florida, USA; 2005 p 2386.
24. Yu H, Shimakawa A, McKenzie CA, Lu W, Reeder SB, Hinks RS, Brittain JH. Phase and amplitude correction for multi-echo water-fat separation with bipolar acquisitions. J Magn Reson Imaging 2010;31:1264–1271.
25. Lu Y, Lu W. JIGSAW: jJoint Inhomogeneity Estimation via Global Segment Assembly for Water-Fat Separation. IEEE Trans Med Imaging 2011;30:1417–1426.
26. Ren J, Dimitrov I, Sherry AD, Malloy CR. Composition of adipose tissue and marrow fat in humans by 1H NMR at 7 Tesla. J Lipid Res 2008;49:2055–2062.
27. Yu H, Shimakawa A, McKenzie C, Brittain J, Reeder S. IDEAL water-fat decomposition with multipeak fat spectrum modeling, 2008 April, Toronto. p 652.
28. Hamilton G, Yokoo T, Bydder M, Cruite I, Schroeder ME, Sirlin CB, Middleton MS. In vivo characterization of the liver fat (1)H MR spectrum. NMR Biomed 2010 [Epub ahead of print].
29. Westwood M, Anderson LJ, Firmin DN, Gatehouse PD, Charrier CC, Wonke B, Pennell DJ. A single breath-hold multiecho T_2^* cardiovascular magnetic resonance technique for diagnosis of myocardial iron overload. J Magn Reson Imaging 2003;18:33–39.
30. Yu H, Shimakawa A, McKenzie CA, Vu AT, Brau ACS, Beatty PJ, Reeder SB, Brittain JH. A multi-echo acquisition method with reduced echo spacing for robust IDEAL water-fat decomposition at 3T. Proceedings 14h Scientific Meeting, International Society for Magnetic Resonance in Medicine. Berlin, Germany; 2007. p 3353.
31. Tsao J, Jiang Y. Hierarchical IDEAL—robust water-fat separation at high field by multiresolution field map estimation. Proceedings 16th Scientific Meeting, International Society for Magnetic Resonance in Medicine. Toronto, Canada; 2008. p 653.
32. Granlund K, Daniel B, Hargreaves B. Low-resolution spectral cost function for field map estimation. Proceedings 17th Scientific Meeting, International Society for Magnetic Resonance in Medicine. Honolulu, Hawaii, USA; 2009. p 564.